1st International e-Conference
on Energies
14 - 31 March 2014

Conference Proceedings Paper - Energies „Whither Energy Conversion? Present Trends, Current Problems and Realistic Future Solutions"

Performance of a 250 kW Organic Rankine Cycle System for Off-design Heat Source Conditions

Ben-Ran Fu* and Chih-His Liu

Green Energy and Environment Research Laboratories, Industrial Technology Research Institute, Hsinchu, Taiwan; E-Mail: brfu@itri.org.tw (B.R.F.); CHLiu@itri.org.tw (C.H.L.)

* Author to whom correspondence should be addressed; E-Mail: brfu@itri.org.tw (B.R.F.); Tel.: +886-3-591-8637; Fax: +886-3-582-0017.

Abstract: An organic Rankine cycle system with a preheater, evaporator, condenser, turbine, generator, and pump was used to study its off-design performance and operational control strategy. R245fa was used as a working fluid. The net power output is 243 kW and the system thermal efficiency is 9.5% under the design conditions. For an off-design heat source flow rate (m_W), the operating pressure was controlled to meet the condition that the R245fa reached the saturation liquid and vapor states at the outlet of the preheater and evaporator, respectively. The analytical results demonstrated that the operating pressure increased with increasing m_W; a higher m_W yielded better heat transfer performance of the preheater and required a smaller evaporator heat capacity; and the net power output and system thermal efficiency increased with increasing m_W. The net power output increased by 64.0% while the total heat transfer rate increased by only 9.2% for the studied range of m_W. To conclude, an off-design operation is studied for a heat source flow rate which varied from −39.0% to +78.0% from the designed rate, resulting in −29.2% to +16.0% and −25.3% to +12.6% variations in the net power output and system thermal efficiency, respectively.

1. Introduction

An organic Rankine cycle (ORC), in general, employs the same principle as the steam Rankine cycle but uses organic fluids with a low boiling point as the working fluid, which enables power generation for a low heat source temperature [1]. The ORC is considered to be one of the most economic and efficient ways to convert low grade thermal energy, such as geothermal energy, solar thermal energy, waste heat recovery, biomass energy, and ocean thermal energy, to electricity [2]. In recent years, ORCs are being studied in many contexts, including technical-economical-market surveys [1,3], selection of the working fluid [4–6], proof of concept demonstrations [7,8], models for optimal control strategies [9], quasi-dynamic models [10], and running tests of prototypes for ORC systems [11,12].

Because an ORC system provides the heat to power process, the heat exchanger system is a very important component. Moreover, an evaporating temperature related to the working fluid flow rate and the specific enthalpy change is a crucial parameter in an ORC system. Li et al. [13] explored the effect of the evaporating temperature on the system thermal and exergy efficiencies and the net power output of an OCR system. Their results demonstrated that the system exergy efficiency and net power output increases with an increase in the evaporating temperature.

The pinch point temperature difference of the heat exchanger system, another important parameter, also significantly influences the performance of an ORC system. Li et al. [14] found that the optimal pinch point temperature difference of the evaporator is about 13 ℃, while the pinch point temperature of the condenser is about 17 ℃ for the system conditions they studied. Different organic working fluids achieve the maximum net power output per heat transfer area at nearly the same evaporator pinch point temperature. In addition, they also demonstrated that the optimal pinch point temperature difference of the evaporator decreases with a decrease in the pinch point temperature of the condenser.

Although there have been many studies concerning the effect of a number of system parameters on the ORC system performance [2,5,9,13–18], a detailed analysis of the effect of the heat source conditions on the heat transfer characteristics and system performance has rarely been performed. In this work, an analysis study of the heat transfer characteristics and system performance of a 250 kW ORC system at off-design heat source flow rates was conducted by the pressure control approach, i.e., changing the evaporating pressure to meet the particular system requirements when the heat source flow rate varies from the design value. In addition, the evaporating temperature and pinch point temperature difference were also examined for this ORC system.

2. System Description

The ORC system being studied here is depicted in Figure 1; it consisted of a pump, preheater (shell-and-tube type), evaporator (flooded and shell-and-tube type), turbine, generator, condenser (flooded and shell-and-tube type), and hot water (from a boiler with a maximum capacity of 3788 kW) and cooling water (from a cooling tower with a maximum capacity of 1000 RT, i.e., 3860 kW) circulation systems. The design parameters of the preheater are listed in Table 1. In the present study, enhanced factors of 1.6 and 1.2 were employed when estimating the heat transfer coefficients in the shell side and the tube side, respectively, of the preheater. The refrigerant R245fa was used as the working fluid;

this refrigerant is one of the most suitable fluids for low grade waste heat recovery in an ORC system [19]. The mass flow rate (m_R) was set to be 11.58 kg/s. The working fluid R245fa flowed in the shell side of the heat exchangers while hot and cooling water flowed in the tube side. Recently, this ORC prototype, the engineering drawing of which is shown in Figure 2, has been under construction at the Industrial Technology Research Institute, Taiwan.
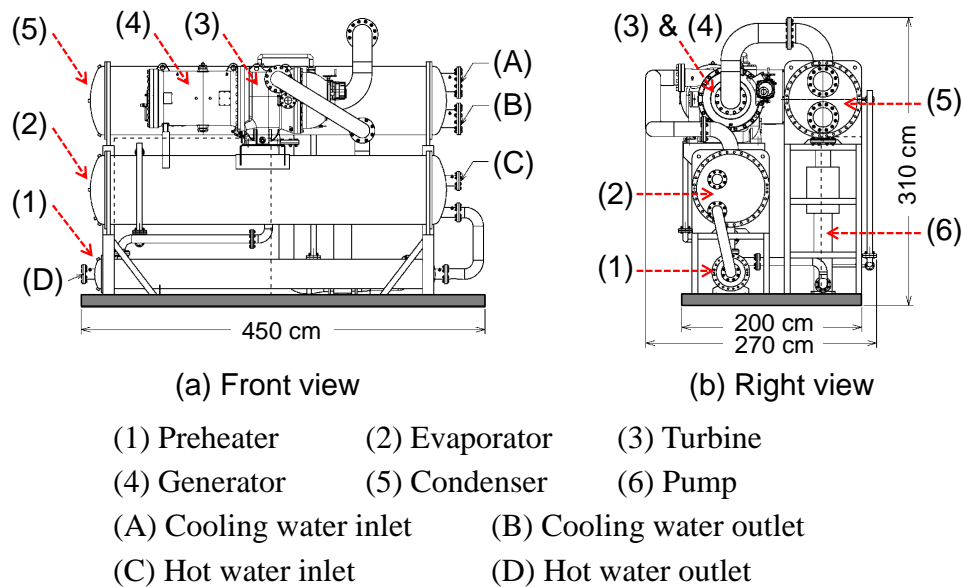
Figure 1. Schematic diagram of the studied ORC system.
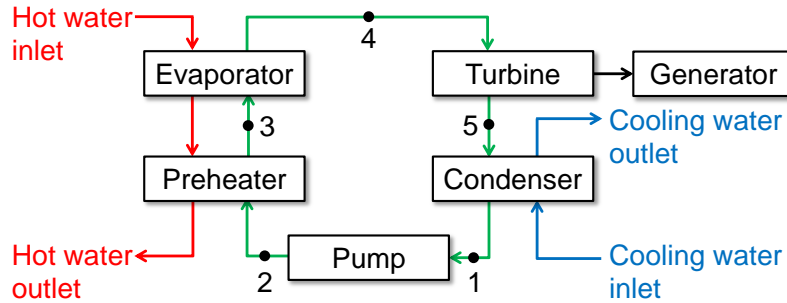
Table 1. Detailed parameters of the designed preheater.

Tube inner/outer diameter	1.471/1.587 cm
Tube thickness	0.058 cm
Tube number	200
Tube in window	83
Tube bundle	1 pass
Tube inner type	Rifled
Tube outer type/Fin per inch (FPI)	Low-finned/42
Tube arrangement	Staggered
Tube pitch transverse	1.984 cm
Tube pitch longitudinal	1.718 cm
Tube/Shell length	360 cm
Shell inner diameter	32.45 cm
Bundle hole diameter	1.61 cm
Bundle diameter	31.66 cm
Sealing strips number	0
Nozzle inner diameter	10 cm
Baffle plate diameter	31.95 cm
Baffle thickness	0.4 cm
Baffle spacing	20 cm
Baffle cut	30%
Baffle plate number	17
Tube side enhanced factor	1.2
Shell side enhanced factor	1.6

Figure 2. Engineering drawing of the ORC prototype: (**a**) Front view and (**b**) Right view.

(a) Front view   (b) Right view

(1) Preheater   (2) Evaporator   (3) Turbine
(4) Generator   (5) Condenser   (6) Pump
(A) Cooling water inlet   (B) Cooling water outlet
(C) Hot water inlet   (D) Hot water outlet

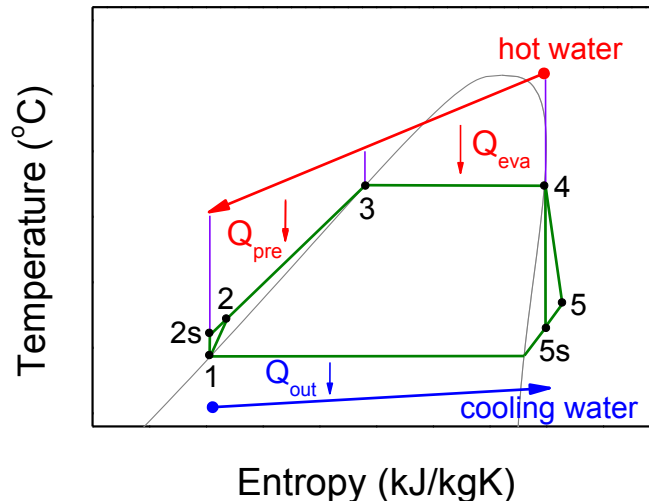**Figure 3.** T-s diagram of the ORC system.

Figure 3 shows the T-s diagram of this ORC system. The design operating pressures of the preheater/evaporator and of the condenser are 1.265 MPa (the evaporation/saturation temperature, $T_{R,eva}$, is 100 °C) and 0.242 MPa (the condensation temperature is 39 °C), respectively. The designed set point for the heat source (hot water) temperature ($T_{w,in}$) and mass flow rate (m_W) are 133.9 °C and 15.39 kg/s, respectively. Under the design conditions, the net power output is 243 kW and the system thermal efficiency is 9.5%. The resultant analyzed heat source flow rate ranged from 9.39 kg/s to 27.39 kg/s.

3. Analysis Methodology

The following assumptions were made for the present analysis. (1) Each component is in the steady state under both flow and thermal conditions. (2) Pressure drops in the heat exchangers (preheater,

evaporator, and condenser) can be neglected. (3) The heat loss in each of the components and in the system pipes can be ignored. (4) The pump, turbine, and generator efficiencies are 90%, 80%, and 90%, respectively. (5) For an off-design flow rate of the heat source, a new operating pressure of the preheater/evaporator has to be chosen to meet the following requirements: R245fa reaches the saturation liquid state at the outlet of the preheater (point 3 in figure 3) and the saturation vapor state at the outlet of the evaporator (point 4 in figure 3), i.e., zero superheating.

The mathematical models of each component as well as of the system performance are presented below in brief. The system thermal efficiency (E_{sys}) can be obtained from the following equations:

$$E_{sys} = W_{net} / Q_{tot} \tag{1}$$

$$W_{net} = W_{out} - W_{in} \tag{2}$$

$$W_{out} = W_{tur} \cdot E_{gen} \tag{3}$$

$$W_{tur} = m_R (h_4 - h_{5s}) \cdot E_{tur} \tag{4}$$

$$W_{in} = m_R (h_{2s} - h_1) / E_{pump} \tag{5}$$

$$E_{tur} = (h_4 - h_5) / (h_4 - h_{5s}) \tag{6}$$

$$E_{pump} = (h_{2s} - h_1) / (h_2 - h_1) \tag{7}$$

$$Q_{tot} = Q_{pre} + Q_{eva} \tag{8}$$

$$Q_{pre} = m_R (h_3 - h_2) = (UA \cdot \Delta T_{lm})_{pre} \tag{9}$$

$$Q_{eva} = m_R (h_4 - h_3) = (UA \cdot \Delta T_{lm})_{eva} \tag{10}$$

$$\frac{1}{U} = \frac{1}{h_R} + \frac{1}{h_W}(\frac{d_o}{d_i}) + \frac{d_o}{2k}\ln(\frac{d_o}{d_i}) \tag{11}$$

Here, W_{net} is the net power output of the system; W_{out} is the power output of the generator; W_{in} is the power requirement of the pump; W_{tur} is the power output of the turbine; h_i is the specific enthalpy for i = 1–5, 2s, and 5s; Q_{tot} is the total heat transfer rate of the preheater and evaporator; Q_{pre} is the heat transfer rate of the preheater; Q_{eva} is the heat transfer rate of the evaporator; m_R is the mass flow rate of the working fluid, i.e., R245fa; E_{gen}, E_{tur}, and E_{pump} are the efficiencies of the generator, turbine, and pump, respectively; U is the overall heat transfer coefficient; A is the total heat transfer area; ΔT_{lm} is the logarithmic mean temperature difference (LMTD); h_R and h_W are the heat transfer coefficients of the shell side (R245fa side) and tube side (water side), respectively, of the heat exchanger; d_o and d_i are the outer and the inner diameters, respectively, of the tube; and k is the thermal conductivity of the tube.

Moreover, in this study the heat transfer functioning of the preheater was calculated by the classical effectiveness–NTU method [20]; and the Bell–Delaware method [21] (equation (12)) and the Gnielinski correlation [22] (equation (13)) were employed to calculate the heat transfer coefficients of the shell and tube sides, respectively, of the designed shell-and-tube preheater:

$$h_R = h_0 \cdot J_c \cdot J_l \cdot J_b \cdot J_s \cdot J_r \tag{12}$$

$$h_W = \frac{(f/2)(\text{Re}-1000)\,\text{Pr}}{1+12.7\sqrt{f/2}\,(\text{Pr}^{2/3}-1)}\left(\frac{k}{d_i}\right) \tag{13a}$$

$$f = (1.58\ln\text{Re} - 3.28)^{-2} \tag{13b}$$

where h_0 is the heat transfer coefficient for an ideal tube bundle; J_c, J_l, J_b, J_s, and J_r are the correction factors for the baffle cut, baffle leakage effects, bundle bypass flow, laminar flow, and unequal baffle spacing, respectively, in the inlet and outlet sections; f is the friction factor; Re is the Reynolds number; and Pr is the Prandtl number.

4. Results and Discussion

Figure 4 shows the analytical results of the operating pressure (P_R), and evaporation/saturation temperature ($T_{R,eva}$) as a function of the heat source flow rate (m_W). As shown in Figure 4, the operating pressure and evaporation temperature increased from 0.775 MPa to 1.675 MPa and from 79.3 ℃ to 113.2 ℃, respectively, as the heat source flow rate increased from 9.39 kg/s to 27.39 kg/s. Both P_R and $T_{R,eva}$ increased rapidly for $m_W < 17.39$ kg/s and gradually for $m_W \geq 17.39$ kg/s. Thus, the present results can be used as a guideline for this system when choosing the operating pressure and evaporation temperature for off-design heat source flow rates.

Figure 4. Operating pressure and evaporation temperature as a function of the heat source flow rate.
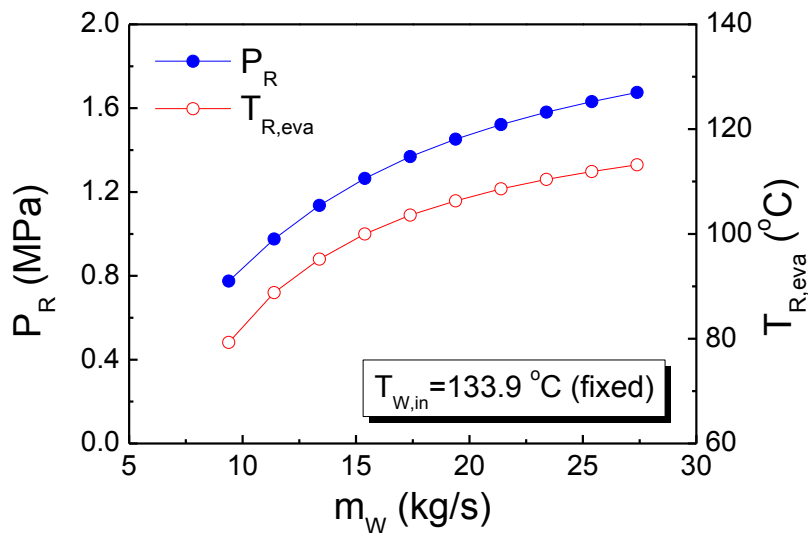

Figure 5 shows the temperature distribution of hot water and R245fa for three different heat source flow rates. Case (b) in Figure 5 is the design condition of this study. As m_W increased, the inlet temperature of the compressed fluid state R245fa (point 2 in Figure 3) increased slightly from 39.3 ℃ to 39.7 ℃ (due to the different operating pressures in the preheater and evaporator) and the outlet temperature of the hot water increased from 72.9 ℃ to 110.9 ℃. In addition, this figure also illustrates that the minimum temperature difference between the hot and cold streams occurred at the middle point between the preheater and evaporator. This particular location is considered to be the pinch point of the heat exchanger system. The pinch point temperature differences for cases (a), (b), and (c) are

10.1 ℃, 10.1 ℃, and 8.8 ℃, respectively. This indicates that for this system the pinch point temperature difference was not significantly affected by m_W. In previous work by Wang et al. [23], the optimal pinch point temperature difference at the evaporator was recommended to be ≤ 15 ℃ when the heat source temperature in an ORC system is between 100 ℃ and 220 ℃. Their results also demonstrated that a higher pinch point temperature difference leads to a decrease of the total net power output of an ORC system. Moreover, for engineering applications, the acceptable range of the pinch point temperature difference was 6 ℃ to 20 ℃ [24]. Therefore, when considering the ORC system performance, the pinch point temperature differences of the present heat exchanger system might be suitable for such applications.

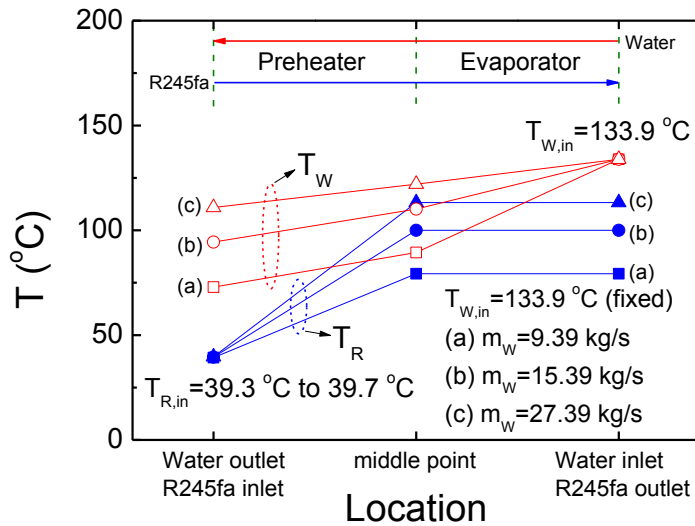**Figure 5.** Temperature distribution of hot water and R245fa for different heat source flow rates.

Figure 6 shows the heat transfer rate of the preheater (Q_{pre}) and the evaporator (Q_{eva}) as a function of the heat source flow rate. In this figure, the total heat transfer rate (Q_{tot}) is the sum of Q_{pre} and Q_{eva}. It is clearly shown that Q_{pre} increased from 654 kW to 1258 kW but Q_{eva} decreased from 1773 kW to 1392 kW with an increase in m_W. This figure also demonstrates that the increase of Q_{pre} was larger than that of Q_{eva}. As a result, the total heat transfer rate increased from 2427 kW to 2650 kW with an increase in m_W. In addition, the change rates of Q_{pre}, Q_{eva}, and Q_{tot} for $m_W < 17.39$ kg/s were significantly higher than that for $m_W \geq 17.39$ kg/s. In summary, Figure 6 indicates that a higher heat source flow rate resulted in a better heat transfer performance of the designed preheater and required a smaller evaporator heat capacity.

Figure 7 shows the heat transfer coefficient (h or U) of the preheater as a function of the heat source flow rate. This figure illustrates that as m_W increased, the heat transfer coefficient of the tube side ($h_{W,pre}$) increased rapidly from 3362 W/m²K to 9162 W/m²K, i.e., increasing by 272.5%, and at an almost constant increase rate. On the other hand, the heat transfer coefficient of the shell side ($h_{R,pre}$) remained nearly constant at about 815 W/m²K. In addition, because the heat transfer coefficient of the shell side was much smaller than that of the tube side, the overall heat transfer coefficient (U_{pre}) increased gradually from 308 W/m²K to 373 W/m²K, i.e., increasing by only 21.1%. The increase of

Q_{pre}, as shown in Figure 6, resulted from the increase of the overall heat transfer coefficient and logarithmic mean temperature difference (LMTD, ΔT_{lm}), as shown in Figure 7. ΔT_{lm} increased from 19.6 °C to 29.9 °C, i.e., increasing by 52.6%, for the studied range of m_W values.

Figure 6. Heat transfer rate as a function of the heat source flow rate.
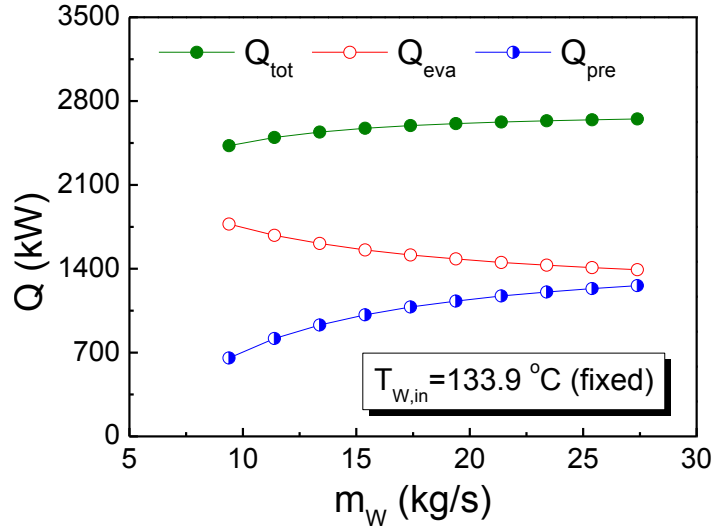

Figure 7. Heat transfer coefficient of the preheater as a function of the heat source flow rate.
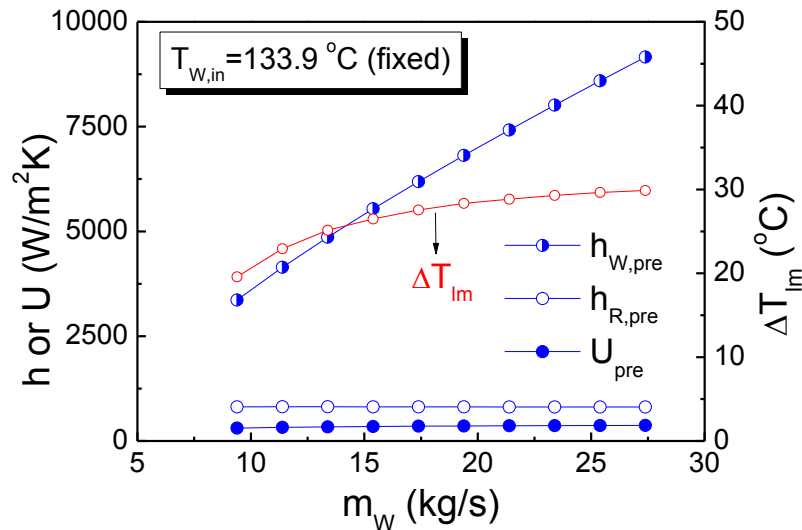
Most importantly, these results further demonstrate that the net power output (W_{net}) and system thermal efficiency (E_{sys}) increased from 172 kW to 282 kW and from 7.1% to 10.7%, respectively, with an increase in m_W, as shown in Figure 8. The result also illustrates that the power requirement for the pump (W_{in}) is 5.5 kW to 14.4 kW, which is only about 3.2% to 5.1% of the power output of the generator (W_{out}). Moreover, it is worth mentioning that for the studied range of m_W values, the net power output increased by 64.0% (from 172 kW to 282 kW) while the total heat transfer rate (Q_{tot}) increased by only 9.2% (from 2427 kW to 2650 kW). This result indicates that the system performance

was significantly enhanced by increasing m_W. It is also interesting to note that W_{net}, W_{out}, W_{in}, and E_{sys} increased rapidly for $m_W < 17.39$ kg/s but gradually for $m_W \geq 17.39$ kg/s, which is similar to the characteristics of P_R and $T_{R,eva}$, as shown in Figure 4. The trend of these results can be used as a prediction reference for the present system when using off-design heat source flow rates. Finally, it is shown that for an off-design operation, a pressure control approach within a −39.0% to +78.0% heat source flow rate variation from the designed parameters resulted in −29.2% to +16.0% and −25.3% to +12.6% variations in the net power output and system thermal efficiency, respectively.

Figure 8. Net power output and system efficiency as a function of the heat source flow rate.
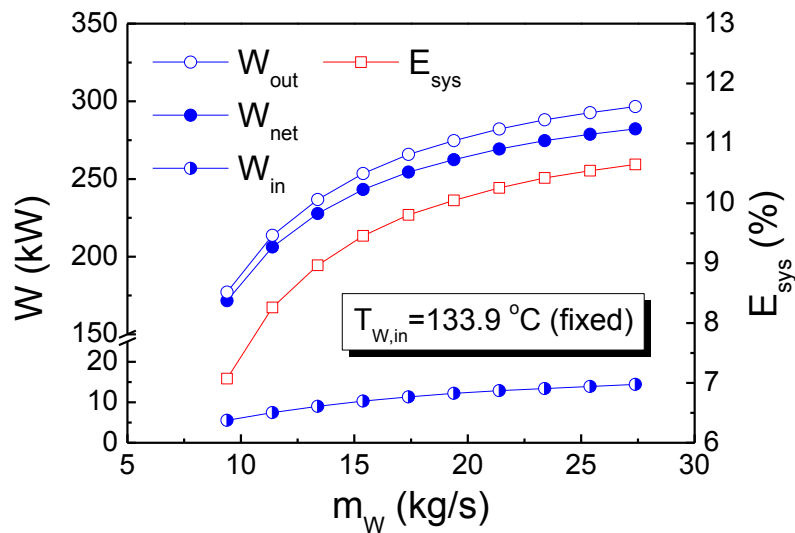
5. Summary and Conclusions

In this paper, an analysis study of the effect of the heat source flow rate on the heat transfer characteristics of a preheater and the system performance of a 250 kW organic Rankine cycle (ORC) system was conducted. The refrigerant R245fa was used as a working fluid, with a constant flow rate of 11.58 kg/s. The design conditions for the operating pressures of the preheater/evaporator and the condenser are 1.265 MPa (i.e., evaporation temperature of 100 ℃) and 0.242 MPa (i.e., condensation temperature of 39 ℃), respectively. The analyzed heat source flow rate (m_W) ranged from 9.39 kg/s to 27.39 kg/s with a constant inlet temperature of 133.9 ℃. The efficiencies of the pump, turbine, and generator were assumed to be 90%, 80%, and 90%, respectively. The net power output is 243 kW and the system thermal efficiency is 9.5% under the design conditions.

For an off-design heat source flow rate, a new operating pressure of the preheater/evaporator was chosen to meet the following limitation: R245fa reaches the saturation liquid state at the outlet of the preheater and the saturation vapor state at the outlet of the evaporator, i.e., zero superheat. The analytical results demonstrated that (1) the operating pressure of the preheater/evaporator increased from 0.775 MPa to 1.675 MPa (i.e., the evaporation temperature increased from 79.3 ℃ to 113.2 ℃) with an increase in m_W; (2) a higher m_W yielded better heat transfer performance of the preheater and required a smaller heat capacity of the evaporator; (3) the pinch point temperature differences (8.8 ℃ to 10.4 ℃) of this ORC system were appropriate from a system performance point of view [23,24];

and (4) the net power output and system thermal efficiency increased with an increase in m_W, especially for $m_W < 17.39$ kg/s. Most importantly, these results illustrated that the net power output increased by 64.0% while the total heat transfer rate increased only by 9.2% for the studied range of m_W values. This result indicates that the performance of this system was significantly improved by increasing m_W. In conclusion, an off-design operation of this ORC system is studied with a pressure control approach for a heat source flow rate which varied by −39.0% to +78.0% from the designed rate, resulting in −29.2% to +16.0% and −25.3% to +12.6% variations in the net power output and system thermal efficiency, respectively.

Acknowledgments

Conflicts of Interest

The authors declare no conflict of interest.

References

1. Quoilin, S.; Broek, M.V.D.; Declaye, S.; Dewallef, P.; Lemort, V. Techno-economic survey of Organic Rankine Cycle (ORC) systems. *Renewable and Sustainable Energy Reviews* **2013**, *22*, 168–186.
2. Wang, J.; Yan, Z.; Wang, M.; Maa, S.; Dai, Y. Thermodynamic analysis and optimization of an (organic Rankine cycle) ORC using low grade heat source. *Energy* **2013**, *49*, 356–365.
3. Vélez, F.; Segovia, J.J.; Martín, M.C.; Antolín, G.; Chejne, F.; Quijano, A. A technical, economical and market review of organic Rankine cycles for the conversion of low-grade heat for power generation. *Renewable and Sustainable Energy Reviews* **2012**, *16*, 4175–4189.
4. Bao, J.; Zhao, L. A review of working fluid and expander selections for organic Rankine cycle. *Renewable and Sustainable Energy Reviews* **2013**, *24*, 325–342.
5. Micheli, D.; Pinamonti, P.; Reini, M.; Taccani, R. Performance analysis and working fluid optimization of a cogenerative organic rankine cycle plant. *Journal of Energy Resources Technology – Transactions of the ASME* **2013**, *135*, 021601.
6. Rayegan, Y.; Tao, Y.X. A procedure to select working fluids for Solar Organic Rankine Cycles (ORCs). *Renewable Energy* **2011**, *36*, 659–670.
7. Aghahosseini, S.; Dincer, I. Comparative performance analysis of low-temperature Organic Rankine Cycle (ORC) using pure and zeotropic working fluids. *Applied Thermal Engineering* **2013**, *54*, 35–42.
8. Garg, P.; Kumar, P.; Srinivasan, K.; Dutta, P. Evaluation of carbon dioxide blends with isopentane and propane as working fluids for organic Rankine cycles. *Applied Thermal Engineering* **2013**, *52*, 439–448.
9. Manente, G.; Toffolo, A.; Lazzaretto, A.; Paci, M. An Organic Rankine Cycle off-design model for the search of the optimal control strategy. *Energy* **2013**, *58*, 97–106.

10. Bamgbopa, M.O.; Uzgoren, E. Quasi-dynamic model for an organic Rankine cycle. *Energy Conversion and Management* **2013**, *72*, 117–124.

11. Kuo, C.R.; Hsu, S.W.; Chang, K.H.; Wang, C.C. Analysis of a 50 kW organic Rankine cycle system. *Energy* **2011**, *36*, 5877–5885.

12. Lee, Y.R.; Kuo, C.R.; Wang, C.C. Transient response of a 50 kW organic Rankine cycle system. *Energy* **2012**, *48*, 532–538.

13. Li, W.; Feng, X.; Yu, L.J.; Xu, J. Effects of evaporating temperature and internal heat exchanger on organic Rankine cycle. *Applied Thermal Engineering* **2011**, *31*, 4014–4023.

14. Li, Y.R.; Wang, J.N.; Du, M.T.; Wu, S.Y.; Liu, C.; Xu, J.L. Effect of pinch point temperature difference on cost-effective performance of organic Rankine cycle. *International Journal of Energy Research* **2013**, *39*, 1952–1962.

15. Delgado-Torres, A.M.; García-Rodríguez, L. Analysis and optimization of the low-temperature solar organic Rankine cycle (ORC). *Energy Conversion and Management* **2010**, *51*, 2846–2856.

16. Wang, D.; Ling, X.; Peng, H.; Liu, L.; Tao, L.L. Efficiency and optimal performance evaluation of organic Rankine cycle for low grade waste heat power generation. *Energy* **2013**, *50*, 343–352.

17. Marion, M.; Voicu, I.; Tiffonnet, A.L. Study and optimization of a solar subcritical organic Rankine cycle. *Renewable Energy* **2012**, *48*, 100–109.

18. Roy, J.P.; Mishra, M.K.; Misra, A. Parametric optimization and performance analysis of a waste heat recovery system using Organic Rankine Cycle. *Energy* **2010**, *35*, 5049–5062.

19. Wang, E.H.; Zhang, H.G.; Fan, B.Y.; Ouyang, M.G.; Zhao, Y.; Mu, Q.H. Study of working fluid selection of organic Rankine cycle (ORC) for engine waste heat recovery. *Energy* **2011**, *36*, 3406–3418.

20. Bejan, A. *Heat Transfer*; Wiley: New York, 1993, Chapter 9.

21. Bell, K.J. *Final report of the cooperative research program on shell and tube heat exchangers*, Bulletin No. 5; University of Delaware Engineering Experiment Station: Newark, Delaware, 1963.

22. Gnielinski, V. New equation for heat and mass transfer in turbulent pipe and channel Flow. *International Journal of Chemical Engineering* **1976**, *16*, 359–368.

23. Wang, Z.Q.; Zhou, N.J.; Guo, J.; Wang, X.Y. Fluid selection and parametric optimization of organic Rankine cycle using low temperature waste heat. *Energy* **2012**, *40*, 107–115.

24. Wang, J.; Yan, Z.; Wang, M.; Maa, S.; Dai, Y. Thermodynamic analysis and optimization of an (organic Rankine cycle) ORC using low grade heat source. *Energy* **2013**, *49*, 356–365.